The Astrophysical Journal, 963:122 (11pp), 2024 March 10 https://doi.org/10.3847/1538-4357/ad1bef

Low-mass Stars: Their Protoplanetary Disk Lifetime Distribution

Susanne Pfalzner[1,2] and Furkan Dincer[1,3]
[1] Jülich Supercomputing Center, Forschungszentrum Jülich, D-52428 Jülich, Germany; s.pfalzner@fz-juelich.de
[2] Max-Planck-Institut für Radioastronomie, Auf dem Hügel 69, D-53121 Bonn, Germany
[3] RWTH Aachen, Aachen, Germany
Received 2023 November 17; revised 2024 January 5; accepted 2024 January 6; published 2024 March 6

Abstract

While most protoplanetary disks lose their gas within less than 10 Myr, individual disk lifetimes vary from <1 Myr to ≫20 Myr, with some disks existing for 40 Myr. Mean disk half-lifetimes hide this diversity; only a so-far nonexisting disk lifetime distribution could capture this fact. The benefit of a disk lifetime distribution would be twofold. First, it would provide a stringent test on disk evolution theories. Second, it could function as an input for planet formation models. Here, we derive such a disk lifetime distribution. We heuristically test different standard distribution forms for their ability to account for the observed disk fractions at certain ages. We here concentrate on the distribution for low-mass stars (spectral types M3.7–M6, $M_s \approx 0.1$–$0.24\ M_{\odot}$) because disk lifetimes depend on stellar mass. A Weibull-type distribution ($k = 1.78$, $\lambda = 9.15$) describes the observational data if all stars have a disk at a cluster age $t_c = 0$. However, a better match exists for lower initial disk fractions. For $f(t{=}0) = 0.65$, a Weibull distribution ($k = 2.34$, $\lambda = 11.22$) and a Gaussian distribution ($\sigma = 9.52$, $\mu = 9.52$) fit the data similarly well. All distributions have in common that they are wide, and most disks are dissipated at ages >5 Myr. The next challenge is to quantitatively link the diversity of disk lifetimes to the diversity in planets.

Unified Astronomy Thesaurus concepts: Protoplanetary disks (1300); Planet formation (1241)

1. Introduction

Planets form from the gas and dust disks surrounding young stars. After some time, the gas in the disks dissipates, basically stopping the planets from accreting additional gas. Therefore, the length of the period available for the planets to build up is a crucial parameter for planet formation theory.

There is ample observational evidence that disks develop over time. For example, the mean millimeter dust mass of disks decreases with the age of the star-forming region (e.g., Ansdell et al. 2017; Andrews 2020). Eventually, processes like photoevaporation, winds, and dust growth (e.g., Williams & Cieza 2011; Ercolano & Pascucci 2017; Kunitomo et al. 2020) lead to complete disk dissipation. Consequently, the disk fraction in star-forming regions decreases with cluster age. This decline is visible for diverse disk indicators, such as infrared (IR) excess or accretion signatures (Haisch et al. 2001; Hernández et al. 2007; Fedele et al. 2010; Ribas et al. 2014; Richert et al. 2018).

Haisch et al. (2001) introduced a method of determining the disk lifetime from the decline of the disk fraction with cluster age. While they used a linear fit to their data, exponential fits became the norm as more data became available. Different studies differ in the resulting median disk lifetime from $f_d = 1$–3 Myr (Haisch et al. 2001; Hernández et al. 2008; Fedele et al. 2010; Ribas et al. 2014; Richert et al. 2018; Briceño et al. 2019) to $f_d = 5$–10 Myr (Pfalzner et al. 2014; Ribas et al. 2015; Michel et al. 2021; Pfalzner et al. 2022). The differences mainly result from the different selection criteria for the included clusters and the different methods and evolutionary models used to estimate the ages of the clusters.

While determining a median disk lifetime demonstrated that planets form relatively fast, the limitations of this method have begun to show. Several relatively old disks (>10 Myr) have recently been discovered (e.g., Silverberg et al. 2020). Meanwhile, fully formed planets have been reported in much younger systems. The coexistence of short- and long-lived disks strongly indicates that the distribution of disk lifetimes likely is very wide. Thus, the notion of a median disk lifetime has limited use. Here, we demonstrate a method for deriving a disk lifetime distribution from existing disk fraction values. Such a disk lifetime distribution is essential for deepening our understanding of planet formation for two reasons. First, the disk lifetime distribution puts stringent constraints on disk dispersal models. Second, it can shed new light on the diversity of the planet formation processes (Mordasini et al. 2009; Ida & Lin 2010; Mordasini et al. 2012; Forgan & Rice 2013; Schlecker et al. 2022; Emsenhuber et al. 2023).

2. Old Disks and Young Planets

Examples of disks older than 10 Myr are the ∼10 Myr old HD 98800 B (Ronco et al. 2021), and the ∼14 Myr old stars HD 139614, and HD 143006 (Kennedy et al. 2019; Ballabio et al. 2021). Moreover, a few ∼50 Myr old stars exhibit large fractional IR luminosity indicative of a circumstellar disk and simultaneously spectroscopic signs of accretion. Examples are WISE J080822.18-644357.3 in the Carina association (≈45 Myr; Silverberg et al. 2016; Murphy et al. 2018) and the ≈55 Myr old 2MASS J15460752-6258042 (Lee et al. 2020).

Examples of old disks always face the problem of distinguishing between debris and protoplanetary disks. Such a distinction is complicated by the dust in protoplanetary disks being not primordial but subject to a continual cycle of growth and destruction (Wyatt et al. 2015). Nevertheless, many relatively old stars have been confidently identified as being surrounded by protoplanetary disks. Silverberg et al. (2020) and Lee et al. (2020) discovered six more accreting stars of

ages ≈50 Myr. These objects likely represent long-lived, CO-poor primordial disks or "hybrid" disks simultaneously exhibiting debris and primordial-disk features. All these very-long-lived disks have in common that their host is typically an M-type star.

Atacama Large Millimeter/submillimeter Array (ALMA) observations reveal that many disks display ring structures. A popular interpretation is that these ring structures could be caused by planets that have already grown to a substantial size or are pressure bumps (for a summary, see van der Marel & Pinilla 2023). If ring structures are indeed an indicator of an advanced stage of planet formation, then they also point at a wide spread in planet formation timescales. The most prominent two examples of ring-structured disks, HL Tau (<1 Myr) and TW Hydrae (∼10 Myr), differ considerably in their ages.

The term "the disk lifetime," when referring to the median disk lifetime, implicitly implies that disks exist for a typical characteristic period. The above examples make it clear that this is, to some extent, misleading. These detections of protoplanetary disks older than 20 Myr show that a shift toward a description by a disk lifetime distribution is long overdue. Such a disk lifetime distribution quantifies the relative occurrence rate of any disk lifetime, including those of very-short-lived and long-lived disks.

Disk fractions in clusters are known to depend on stellar mass (e.g., Carpenter et al. 2006; Roccatagliata et al. 2011; Yasui et al. 2014; Ribas et al. 2015; Richert et al. 2018). In a given cluster, high-mass stars tend to have considerably lower disk fractions than low-mass stars. Here, we concentrate on low-mass stars to separate the stellar mass dependence from the intrinsic spread in disk lifetimes. Looking only at low-mass stars (spectral types M3.7–M6, $M_s \approx 0.1$–$0.24\ M_\odot$; Luhman 2023a, and references therein), we will see that the extensive spread in disk lifetimes persists. We chose this particular mass bin because it shows the highest disk fraction at all ages and is still 90% complete for the investigated clusters (see Section 5.1).

3. Toward a Disk Lifetime Distribution

The starting point for determining the disk lifetime distribution is the disk fractions in clusters of different ages. The disk fraction, $f_d(t)$, declines by the number of disks that have reached the end of their lifetime as

$$f_d(t) = f_d(t=0) - \int_0^t T_d\,dt, \tag{1}$$

where T_d denotes the individual disk lifetime and $f_d(0)$ the initial disk fraction, which might be 100% or less. If each star is surrounded by a disk at cluster age ($t = 0$), this simplifies to $f_d(t) = 1 - \int_0^t T_d(t)\,dt$. The disk lifetime distribution is

$$T_d(t) = -\frac{d}{dt} f_d(t). \tag{2}$$

The problems in determining $T_d(t)$ are (i) the uncertainties in cluster ages and disk fractions, resulting in a considerable scatter among the data points, and (ii) the underrepresentation of clusters older than 4 Myr. Unfortunately, linear and exponential fits to the decline in disk fraction with cluster age lead to counterintuitive disk lifetime distributions.

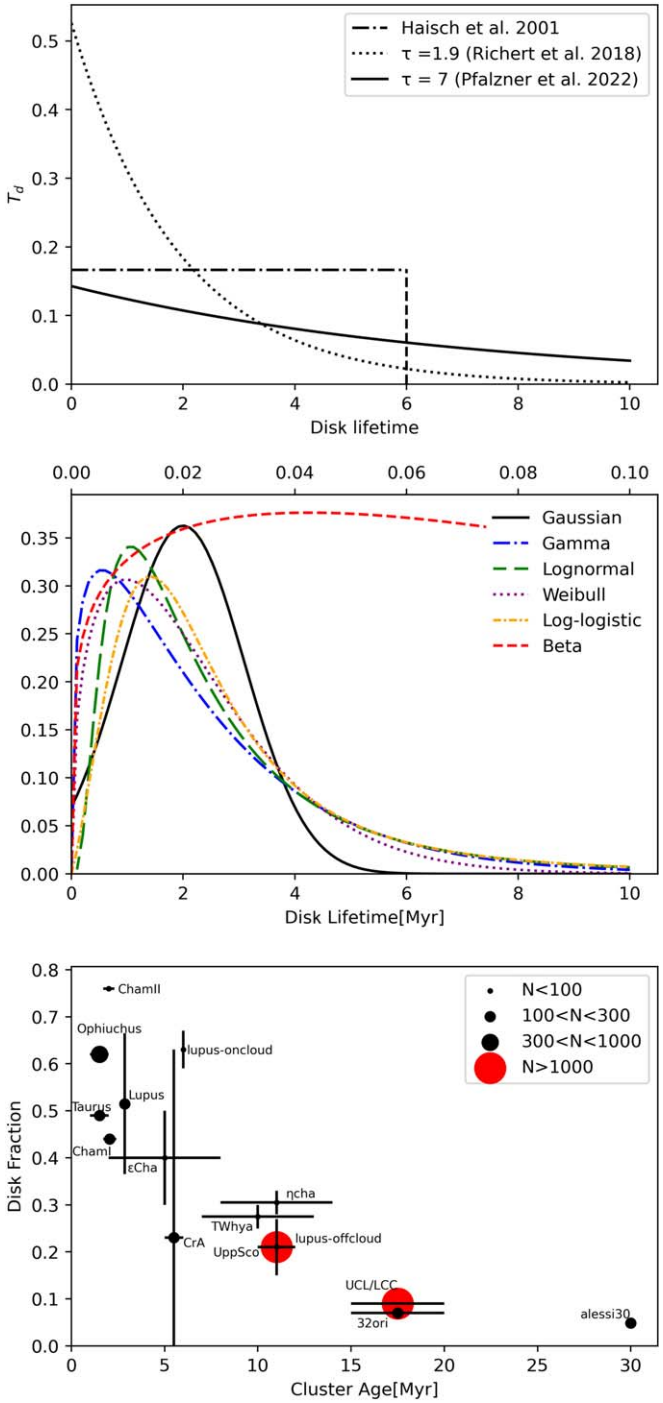

Figure 1. Top: disk lifetime distributions corresponding to the linear fits of the disk fraction vs. age by Haisch et al. (2001, black) and the exponential fits applied by Richert et al. (2018, blue) and Pfalzner et al. (2022, red). Middle: schematic illustration of the distributions tested here. Bottom: illustration of the data points' relative significance due to the given cluster's number of stars. Only clusters within a distance $d < 200$ pc from the Sun are shown.

Haisch et al. (2001) connected an assumed 100% initial disk fraction to the time when all disks seemed to have vanished (6 Myr) by a linear fit. The corresponding disk lifetime distribution is $T_d(t) = 1/6$ (see Figure 1, top panel). This constant distribution would imply that a disk is as likely to disperse at an age of 0.01 Myr as at 6 Myr. Such independence of age is conceptually unsatisfying. The idea of a typical disk

lifetime reflects the expectation of a distribution that shows a clear maximum. A constant disk mass distribution fails to provide such a maximum in the distribution.

As more cluster disk fractions became available, it grew apparent that a linear fit was unsuitable. The question is whether the exponential fits used afterwards for the disk fraction lead to a more realistic disk lifetime distribution. In this case, the disk lifetime distribution would also be an exponential function and of the form

$$T_d(t) = \tau \exp(-t/\tau). \quad (3)$$

This implies that disks are more likely to be dispersed when they are very young (<0.5 Myr) than when they are older (see Figure 1, top panel). For example, the exponential fit given by Richert et al. (2018) would imply that about 2.5 times more disks disperse when they are <0.5 Myr old than when they are 2–2.5 Myr old. For the exponential given in Pfalzner et al. (2022), the dominance of very early disk destruction is less severe; however, like any exponential fit, it also suffers from the problem that very young disks are the ones most likely to be dispersed, and there exists no maximum in the distribution being representative for a typical disk lifetime.

In the following, we systematically test the ability of different distribution functions to represent a disk lifetime distribution. When fitting the various functions to data, one must avoid biases and selection effects in the data as much as possible. Determined median disk lifetimes are very sensitive to cluster selection (Michel et al. 2021; Pfalzner et al. 2022). In particular, including many distant clusters in the sample leads to shorter apparent disk lifetimes. The reason is a selection bias toward higher-mass stars, which disperse their disks earlier than low-mass stars. Therefore, we consider only disk fractions of nearby (<200 pc) clusters and comoving groups as given in Pfalzner et al. (2022).

We consider the different statistical significance of the various data points. Disk fractions determined for clusters containing only a few dozen stars are intrinsically more prone to errors than those from clusters consisting of thousands of stars. In most figures, the size of the symbol scales with the number of stars used to determine the disk fraction to illustrate that we account for the statistical significance of the observational data points (see, e.g. Figure 1, bottom panel). In the following, we refer to this as sample L1++. It contains the clusters Cham I and Cham II (Galli et al. 2021a), Ophiuchus and Taurus (Oph and Tau; Manzo-Martínez et al. 2020), Lupus-on-cloud and Lupus-off-cloud (Spezzi et al. 2015), Lupus (Lup) and Alessi 30 (Galli et al. 2021a; Michel et al. 2021), ϵ Cha (Dickson-Vandervelde et al. 2021; Michel et al. 2021), Corona Australis (CrA), TW Hydra (TW Hya) and Eta Chamaeleontis (η Cha; Dickson-Vandervelde et al. 2021), and Upper Scorpius (Upp Sco) and Upper Centarus-Lupus/Lower Centarus-Crux (UCL/LCC; Luhman & Esplin 2020; Luhman 2022b). The clusters' disk fractions can be found in Table 2 in the Appendix. Our sample's most significant disk fraction data points are those of Upper Sco and UCL/LLC. Furthermore, all data points are affected by errors in the disk fraction and the cluster's age. These uncertainties must be considered appropriately when determining the disk lifetime distribution.

Table 1
Parameters for Gaussian Fits

ID	$f_{\rm USco}$	$f_{\rm U/L}$	$t_{\rm USco}$	$t_{\rm U/L}$	$\bar{t_d}$	$\sigma(t_d)$
$L1_{100}$	0.25	0.09	11.0	15.0	6.95	6.0
$L2_{100}$	0.22	0.09	11.0	17.0	2.85	10.55
$L3_{100}$	0.25	0.09	12.0	15.0	8.96	4.5
$L4_{100}$	0.22	0.11	11.0	15.0	4.20	8.8
$L5_{100}$	0.22	0.09	11.0	15.0	5.7	7.0
L1++	0.25	0.09	11.0	15.0	6.16	6.78

Notes. Here Column (1) indicates the model identifier, $f_{\rm USco}$ stands for the assumed disk fraction of Upper Sco, $f_{\rm U/L}$ for the disk fraction of UCL/LCC, $t_{\rm USco}$ the cluster age of Upper Sco, $t_{\rm U/L}$ that of UCL/LLC, $\bar{t_d}$ the median age of the best-fit distribution, and $\sigma(t_d)$ its standard deviation. L1++ is the best fit when the clusters in Pfalzner et al. (2022) with $d < 200$ pc are considered in addition.

3.1. Gaussian Distribution

First, we fit a Gaussian distribution to the observational data points of Upper Sco and UCL/LLC (see also Pfalzner 2022). We use this case to illustrate the general method. The shape of a Gaussian can be fully determined if two points are given. The two values we base our estimate on are the disk fractions and ages of Upper Sco (Luhman & Esplin 2020) and UCL/LCC (Luhman 2022a; see Table 1, model L1). As mentioned, we use the values for the low-mass stars only because the disk lifetime depends on the stellar mass. The fact that disks still surround 25% of all Upper Sco low-mass stars at 11 Myr means that 25% of these stars have a disk lifetime longer than 11 Myr. Equally, 9% of UCL/LCC low-mass stars have a disk lifetime longer than 15 Myr. In other words, 25% of the curve under the Gaussian is at values >11 Myr and 9% of the curve under the Gaussian is at values >15 Myr (see Figure 2, top panel). A Gaussian with a mean of $\mu = 6.95$ and a standard deviation $\sigma = 6$ simultaneously fulfills these two conditions. Thus, for these conditions, we obtain a mean disk lifetime of approximately 7 Myr, with an extensive spread around this mean value.

The disk fractions and the cluster ages are subject to uncertainties. We performed additional Gaussian fits exploring the combinations of extremes in disk fraction and age for Upper Sco and UCL/LLC (see models L2–L5 in Table 1) to test the sensitivity of the result. Depending on the assumed cluster age and disk fraction, the mean disk lifetime varies between 5 and 8 Myr, with all distributions having a standard deviation $\sigma > 4.5$ Myr (see Figure 2, middle panel).

So far, our fit has solely relied on the disk fractions of Upper Sco and UCL/LCC. In Pfalzner et al. (2022), we demonstrated that more distant clusters are often biased toward higher-mass stars. Therefore, we expand our larger sample to only clusters with distances <200 pc (see Table 2). In the following, this larger sample is referred to as model L1++. In Figure 2 (bottom), we show a comparison between the best fit to this larger cluster sample and the distribution based on Upper Sco and UCL/LCC alone. The fit was obtained, taking the sample size into account. It can be seen that both distributions resemble each other closely. Thus, given the still large uncertainties in the data, both distributions are equally suitable.

We test the fit quality ΔD by calculating the mean least-square distance of the data points to the best-fitting curve. When summing these errors, we weigh the data points according to the number of stars n_i used to determine the disk

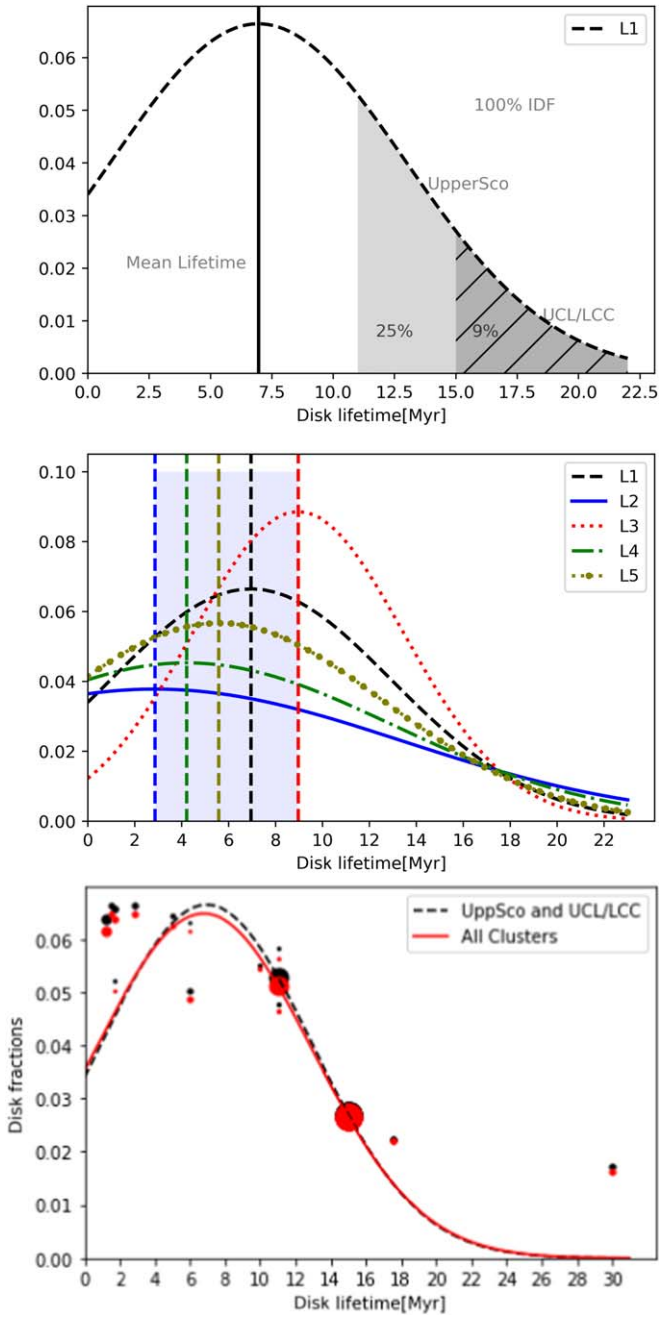

Figure 2. Gaussian-type disk lifetime distributions assuming $f(t=0) = 100\%$. Top: schematics of determining the best-fit curve for model L1. Middle: best fits for data models L1–L5 for data given in Table 1, taking only the data from Upper Sco and UCL/LCC into account. Bottom: comparison between best fits to Upper Sco and UCL/LLC only (black, dashed line) and best fit including clusters with < 200 pc distance (red, full line) given in Table 2. The fit takes the relative sample size into account. The size of the symbol indicates the number of stars in the sample. In all plots the vertical lines indicate the corresponding median disk lifetimes.

fraction,

$$D = \sum_i \frac{n_i}{\sum_i n_i} \sqrt{(\hat{t}_i - t_j)^2 + (\hat{f}_i - f_j)^2},$$

where $\hat{t}_i$ are the cluster ages, $\hat{f}_i$ the cluster disk fraction, and t_j and f_j represent the points on top of the distribution plotted from the initial parameter L1. Figure 2 (bottom) shows the best-fit distributions, considering the additional data points. We can see that the change is only marginal. The reason for this is the relatively small number of stars in these clusters, giving them a low weight in the fit. The best Gaussian disk lifetime distribution is

$$T(t) = \frac{1}{\sqrt{12\pi}} \exp\left[-1/2\left(\frac{t - 6.95}{6}\right)^2\right]. \quad (4)$$

However, there exists a potential problem with a Gaussian distribution. There is a cutoff of the distribution at $t = 0$ Myr, which can be interpreted as a considerable fraction of stars having negative disk lifetimes. Two conclusions exist: (i) the disk fraction distribution has a non-Gaussian shape, and (ii) the initial disk fraction is <100%. In the following, we investigate both options and their combination.

3.2. Tested Types of Distribution

Positively skewed distributions might better represent the disk lifetime distribution while avoiding the problem of negative disk lifetimes. Therefore, we tested the following distributions as possible candidates for the disk lifetime distribution:

$$\text{Gamma: } T(x, \alpha, \beta) = \frac{\beta^\alpha}{\Gamma(\alpha)} x^{\alpha-1} e^{-\beta x},$$

$$\text{Log-normal: } T(x, \sigma, \mu) = \frac{1}{\sqrt{2\pi}\,\sigma x} exp\left(-\frac{[ln(x) - \mu]^2}{2\sigma^2}\right),$$

$$\text{Weibull: } T(x, k, \lambda) = \frac{k}{\lambda}\left(\frac{x}{\lambda}\right)^{k-1} exp\left(-\left(\frac{x}{\lambda}\right)^k\right),$$

$$\text{Log-logistic: } T(x, \alpha, \beta) = \frac{(\beta/\alpha)(x/\alpha)^{\beta-1}}{(1 + (x/\alpha)^\beta)^2},$$

$$\text{Beta: } T(x, p, q) = \frac{\Gamma(p+q)}{\Gamma(p)\Gamma(q)} x^{p-1}(1-x)^{q-1}.$$

See Figure 1 (middle) for a schematic representation of these distributions.

We determine the best fit for all these distribution types to the data of set L1 for Upper Sco and UCL/LLC (see Figure 3, left panel). Table 1 provides the corresponding parameters of these best fits. The equivalent values for models L2–L1++ can be found in Table 5 in the Appendix. In a second step, we determined the deviation from the additional disk fraction data points ΔD. These values are given in Table 4 in the Appendix.

All these distributions start at $f(t=0) = 0$, show a distinct maximum, and have a positively skewed shape. Thus, they seem a more realistic approach than an exponential function. All distributions give remarkably similar results for the disk lifetime distribution. Therefore, using any of these could be justified given the still-existing uncertainties in disk fractions and ages. The mean disk lifetime of these distributions lies in the range 8.1–9.3 Myr. Hence, these values agree with the disk lifetime of ≈8 Myr found by Michel et al. (2021). For left-skewed distributions, the median disk lifetime and the maximum in the distribution differ. This maximum corresponds to the time at which most stars shed their disks. This maximum lies in the 5.8–7.21 Myr range for the best-fit distributions.

Table 2
Disk Fractions

Identification	d (pc)	Age (Myr)	N_{stars}	f_d	Limit	Median mass ($M_\odot$)	$\log(\rho_c)$ ($M_\odot$/pc^3)	Source
Alessi 30	108	30	162	0.049[a]	0.04 $M_\odot$	…	…	(a)
UCL/LLC	150	15–20	3665	0.09 ± 0.01	…	0.15	−0.85 -(−1.05)	(b)
32 Ori	95	15–20	160	$0.07^{+0.03}_{-0.02}$	…	0.15	…	(g)
Upp Sco	145	10–12	1774	$0.22 \pm 0.02/0.20$	0.01 $M_\odot$	0.15	−0.59	(b), (c)
Lupus-off cloud	160	10–12	60	0.21 ± 0.06	0.05 $M_\odot$	…	…	(h)
η Cha	94	8–14	40	$0.28 \pm 0.14/33 \pm 0.16$	…	…	…	(d)
TW Hya	56	7–13	56	$0.25/0.30$, $0.19^{+0.08}_{0.06}$	…	…	…	(d), (j)
Lupus-on cloud	160	6	30	0.63 ± 0.04	0.05 $M_\odot$	…	…	(h)
CrA	152	5	146	0.23 ± 0.4	0.04 $M_\odot$	…	…	(d)
ϵ Cha	101	5 (3–8)	90	0.5/0.3[b]	…	…	…	(d), (e)
Lup	158	2.6–3.1	158	0.50/0.53	0.03 $M_\odot$	…	…	(a), (d)
Cham I	188	1.7	183	0.44	6 <G <20	…	…	(f)
Cham II	197	1.7	41	0.76	G12-G18	…	…	(f)
Tau	128–196	1–2	137	0.49, 0.637	0.05 $M_\odot$	…	…	(i), (l)
Oph	139	1–2	420	0.62	…	…	…	(i)

Notes.
[a] Possibly debris disk fraction.
[b] The disk fraction is much higher in the center than the outskirts (>10 pc) of η Cha.
References: (a) Galli et al. (2021a), (b) Luhman (2022a), (c) Luhman & Esplin (2020), (d) Michel et al. (2021), (e) Dickson-Vandervelde et al. (2021), (f) Galli et al. (2021b), (g) Luhman (2022b), (h) Luhman & Esplin (2020), (i) Manzo-Martínez et al. (2020), (j) Luhman (2023b), (l) Luhman (2023a).

Of all investigated distribution types, we favor the following Weibull distribution:

$$T(t) = 91.57t^{0.78}\exp(-51.44t^{1.78}). \quad (5)$$

This is for two reasons. First, it gives the smallest ΔD value. Second, converting these disk lifetime distributions back into a disk fraction versus cluster age plot (see Figure 3, right panel) shows the lowest discrepancy to the disk fractions younger than 5 Myr. However, at these young ages, the observed disk fractions are lower than expected from any of these distributions. One reason for this could be the assumption that all stars are initially surrounded by a disk. However, this assumption may not be justified.

3.3. Role of Initial Disk Fraction

Michel et al. (2021) obtain much better fits to their data when assuming initial disk fractions of 80% and 65% rather than 100%. They attribute the reason for a <100% disk fraction to the presence of binary stars. Other reasons for the initial disk fraction being less than 100% could be that some stars are born without a disk or lose their disk rapidly (<0.5 Myr; Richert et al. 2018).

Another reason could be the age spread in the cluster. For instance, star formation in the star-forming region of Tau has been ongoing for at least 1–3 Myr (Kenyon & Hartmann 1995). Similarly, across Ori, for disks in isolation, the spread in disk mass is likely related to an age spread (van Terwisga et al. 2022). Thus, even if all stars were initially surrounded by a disk at $t = 0$ Myr, the oldest stars of the distribution may have already lost their disks, leading to $f_d(t = 0) < 100\%$.

Assuming a lower initial disk fraction affects the shape of the disk lifetime distribution. The two bottom rows of Figure 3 show the best-fit solutions assuming an initial disk fraction of 80% and 65%, respectively. Like before, all distributions start at $f(t = 0) = 0$, show a distinct maximum, and have a positively skewed shape. Assuming a lower initial disk fraction leads to the mean disk lifetime of these distributions being slightly higher. For $f_{init} = 80\%$, the mean disk lifetimes are 9.0–10 Myr. The lower D is due to the match to the disk fractions of clusters with ages <5 Myr being better. As before, a Weibull distribution gives the best match. The best-fit parameters are again listed in Table 3.

Figure 4 shows a comparison of the Weibull-type distributions assuming an initial disk fraction of 100% (full line), 80% (dashed line) and 65% (dotted line) as well as the corresponding curves in the disk faction versus cluster age illustration. It can be seen that lower initial disk fractions result in the maximum disk destruction shifting to later times. From $t_{max}(100\%) = 5.8$ Myr in the case of a 100% initial disk fraction, it increases to $t_{max}(80\%) = 7.2$ Myr and $t_{max}(65\%) = 8.83$ Myr for lower initial disk fractions. Correspondingly, the median disk fraction increases from $t_d(100\%) = 8.14$ Myr to $t_d(65\%) = 9.93$ Myr. Nevertheless, the curve for 65% would be better to reconcile with the observed disk fractions for clusters <4 Myr. The D values decrease from $D(10\%) = 0.077$ to $D(65\%) = 0.034$. The best fit for a Weibull distribution assuming an initial disk fraction of 65% is

$$T(t) = 0.209\left(\frac{t}{11.22}\right)^{1.34}\exp\left(-\frac{t}{11.22}^{2.34}\right), \quad (6)$$

Surprisingly, this distribution differs only slightly from the Gaussian distribution for a 65% initial disk fraction (see Figure 5), which is given by

$$T(t) = \frac{1}{\sqrt{12\pi}}\exp\left[-1/2\left(\frac{t - 6.95}{6}\right)^2\right]. \quad (7)$$

Thus, for all practical purposes, both heuristic fits could be used.

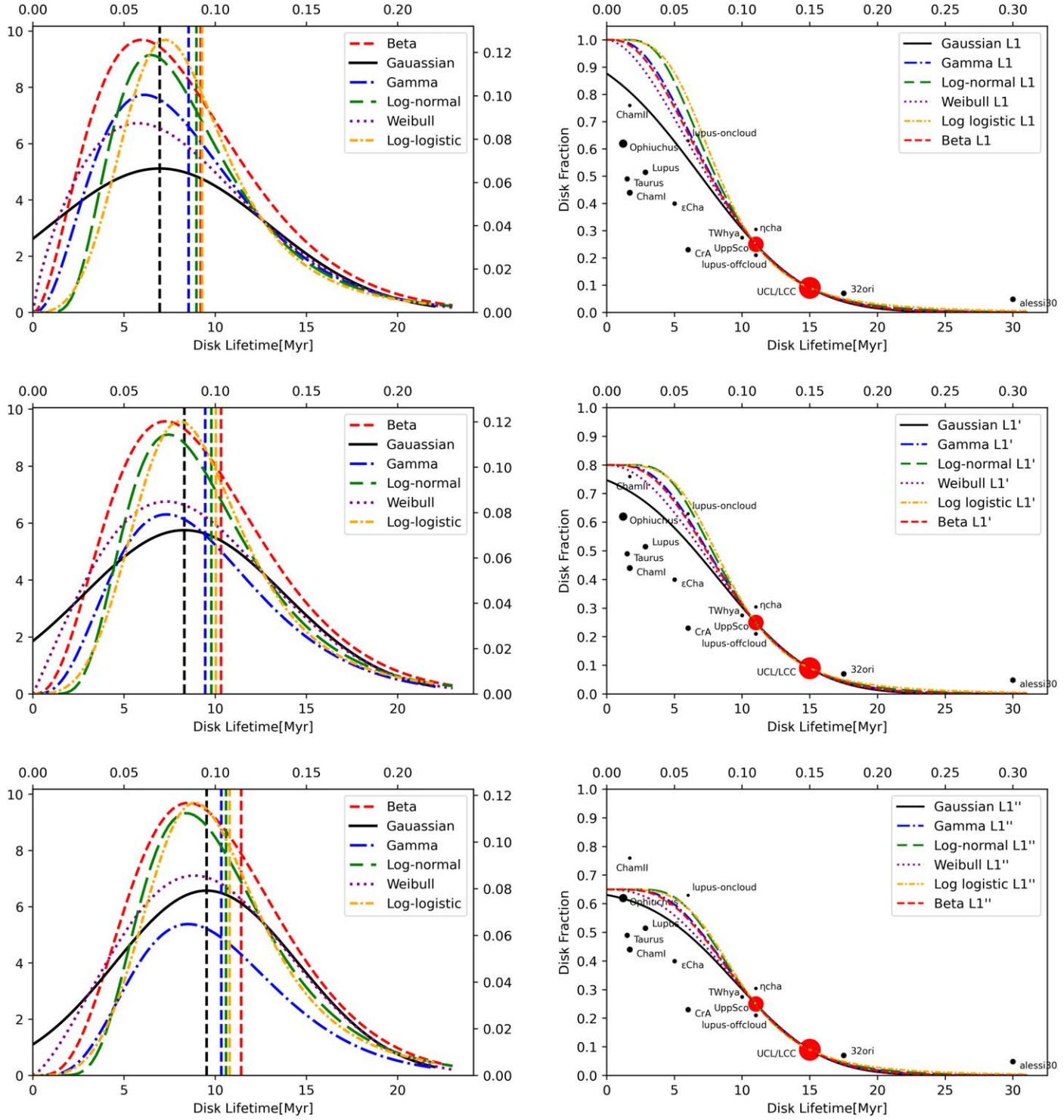

Figure 3. Left column: disk lifetime distributions assuming a gamma, log-normal, Weibull, log-logistic, and beta distribution shape. These fits are based on the L1 data for Upper Sco and UCL/LLC. Right column: corresponding disk fraction vs. cluster age plots assuming the various distributions. The top row shows the results assuming a 100% initial disk fraction, whereas the middle row illustrates the case of an initial disk fraction of 80% and the bottom row for an initial disk fraction of 65%. The vertical lines indicate the corresponding median disk lifetime.

4. Current Limitations

The derived disk lifetime distribution should be regarded as a first iteration step. The challenge is the scarcity of nearby clusters in the age range 5–15 Myr. Our solution was to use the disk fraction of Upper Sco and UCL/LLC as anchor points for determining the disk lifetime distribution. However, there has been a long discussion in the literature concerning the age of Upper Sco. The age determinations in the literature from the last decades fall broadly around two estimates: 5 Myr (de Geus et al. 1989; Preibisch et al. 2002) and 10–12 Myr (Pecaut et al. 2012; Sullivan & Kraus 2021). Here, we used the latter age.

The question is whether it is realistic to attribute Upper Sco and UCL/LLC specific ages. Recent studies of Upper Sco by Ratzenböck et al. (2023) based on new Gaia data show that

Table 3
Parameters for the Different Distribution Types

	$f_{\rm init} = 1.0$				$f_{\rm init} = 0.8$				$f_{\rm init} = 0.65$			
Type	Parameters	t_d	$\sigma(t_d)$	$t_{\rm max}$	Parameters	t_d	$\sigma(t_d)$	$t_{\rm max}$	Parameters	t_d	$\sigma(t_d)$	$t_{\rm max}$
Gaussian	$\sigma = 6.0$ $\mu = 6.95$	6.95	6	6.95	$\sigma = 5.59$ $\mu = 8.22$	8.22	5.59	8.22	$\sigma = 5.04$ $\mu = 9.52$	9.52	5.04	9.52
Gamma	$\alpha = 3.53\beta = 0.41$	8.5	20.6	5.99	$\alpha = 4.47\beta = 0.47$	9.4	19.9	7.31	$\alpha = 5.69\beta = 0.55$	10.32	18.7	8.44
Log-normal	$\sigma = 0.46\mu = 2.08$	8.9	19.4	6.43	$\sigma = 0.43\mu = 2.19$	9.8	19.2	7.40	$\sigma = 0.39$ $\mu = 2.28$	10.59	18.48	8.42
Weibull	$k = 1.78$ $\lambda = 9.15$	8.1	22.4	5.80	$k = 2.03$ $\lambda = 10.21$	9.0	21.7	7.20	$k = 2.34$ $\lambda = 11.22$	9.93	20.29	8.83
Log-logistic	$\alpha = 8.31\beta = 3.92$	9.3	24.8	7.21	$\alpha = 9.08$ $\beta = 4.12$	10.0	25.5	8.04	$\alpha = 9.88$ $\beta = 4.38$	10.78	25.13	8.89
Beta	p=3.02 $q = 32.92$	8.4	20.8	5.97	$p = 3.85$ $q = 37.32$	9.3	20.1	7.27	$p = 4.92$ $q = 43.12$	10.25	18.76	8.52

Notes. Column (1) indicates the distribution type, $f_{\rm init}$ stands for the assumed initial disk fraction, t_d the median disk lifetime, $\sigma(t_d)$ the standard deviation, and $t_{\rm max}$ the maximum of the distribution. The corresponding ΔD values, describing the quality of the fit, can be found in Table 4 in the Appendix.

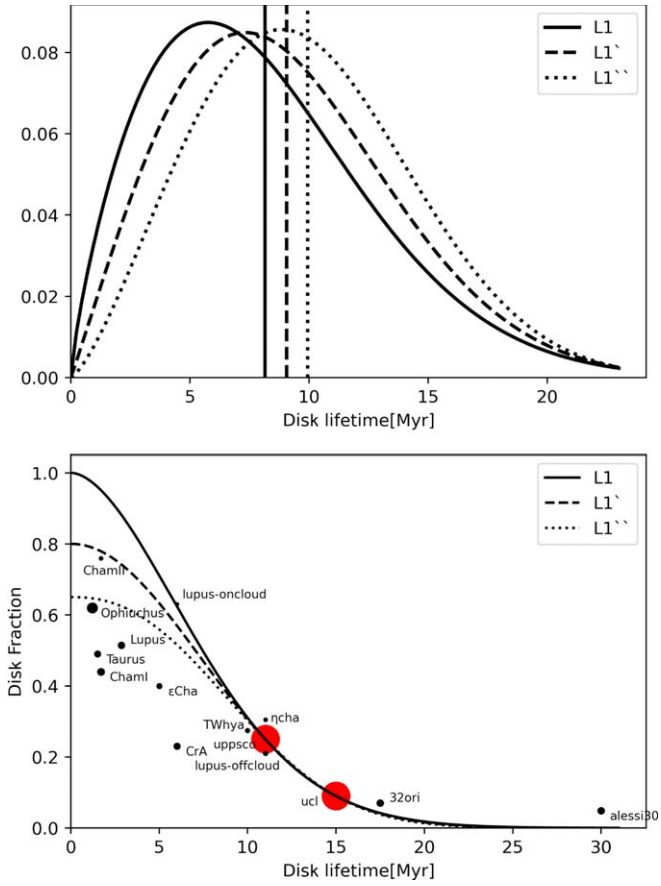

Figure 4. Comparison of Weibull distributions assuming a $f_{\rm init} = 1.00$ (full line), $f_{\rm init} = 0.80$ (dashed line), and $f_{\rm init} = 0.65$ (dotted line) initial disk fraction.

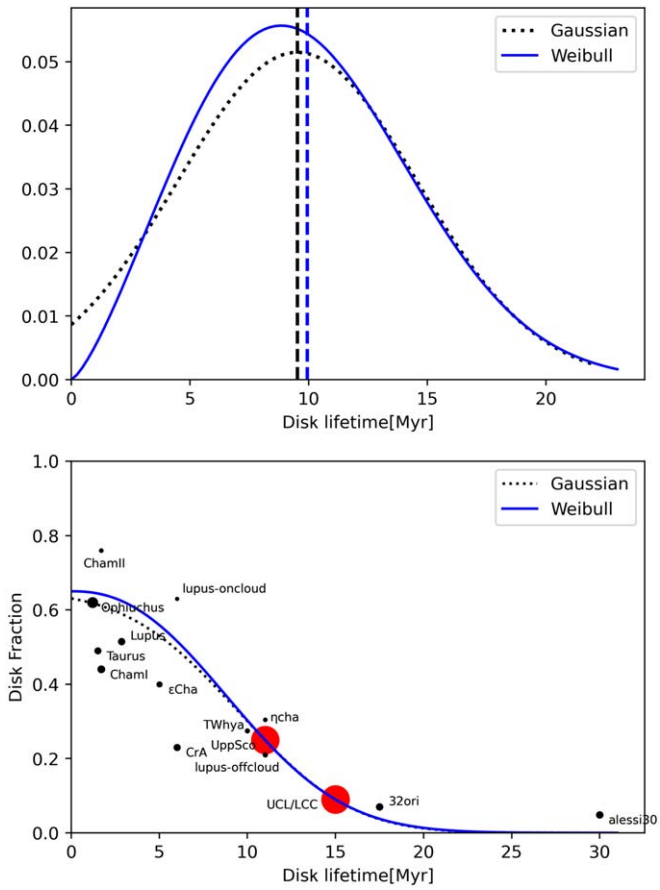

Figure 5. Comparison between Gaussian (dotted line) and Weibull distributions. Top: the distributions. Bottom: corresponding disk fraction vs. cluster age diagram.

Upper Sco's stellar population consists of up to nine subclusters aged between 3 Myr and 19 Myr. However, determining individual ages is also challenging and can be affected by stellar rotation, stellar spots, and photometric variability. The differences in ages of the individual subclusters can explain the wide age spread and the conflicting results in earlier studies. Similarly, the UCL/LCC area can be divided into separate subclusters of different ages. They find that the entire Sco-Cen area is dominated by a brief period of intense star and cluster formation rate about 15 Myr ago, slowly declining since this burst.

As the subclusters in Upper Sco and ULC/LLC have ages roughly in the range of 3–20 Myr, one can obtain disk fractions in this age range. Once these disk fractions are published, one can obtain the next better iteration of the disk lifetime distribution with the method described here.

Determining the initial disk fraction at $t = 0$ is a challenging task. To better understand the influence of the age spread in clusters on disk fractions, it is crucial to make significant efforts in this area. One way of achieving this is by determining the age of individual stars in clusters. This will enable us to put better observational constraints on the $t = 0$ disk fraction in the future.

5. Reasons for the Large Width of the Distribution

The obtained disk lifetime distributions are all very broad ($\sigma > 6$ Myr). It is intriguing to consider the reasons for the vast

differences in disk lifetime, ranging from just 1 Myr to over 20 Myr. Several factors have been identified as potential influencers of individual disk lifetime, including stellar mass, initial disk mass, environment, planet formation, and stellar binarity.

5.1. Stellar Mass

Stellar mass definitely influences the disk lifetime considerably (e.g., Carpenter et al. 2006; Roccatagliata et al. 2011; Yasui et al. 2014; Ribas et al. 2015; Richert et al. 2018; van der Marel & Mulders 2021; Pfalzner et al. 2022). However, we separated this element by restricting our study to low-mass stars of spectral types M3.7–M6 following the classification of Luhman (2022b). They estimate that the contamination is ≈1% and the completeness is ≈90% at spectral types of ⩽M6–M7 for the populations with low extinction in Upper Sco UCL/LCC. Based on a comparison to deeper spectroscopic surveys of Upper Sco, they find that the completeness of the Gaia sample of candidates in that region begins to decrease at spectral types later than M7 (≈0.06 $M_{\odot}$). In this study, all of the populations in Sco-Cen peak for spectral types near M4–M5. This indicates that the populations of Upper Sco and UCL/LLC share similar characteristic masses for their initial mass functions.

The additional clusters used for model L1++ are not restricted to this mass range, because they contain much fewer (apart from Oph, <200) stars than Upper Sco and UCL/LLC. Due to the initial mass function, these clusters are dominated by M- and L-type stars, but some contain also a few early-type stars. Thus, the presence of higher stars (⩾M3) might lower the disk fractions, as the disk lifetime tends to decrease for higher stellar masses. However, due to the dominance of M- and K-type stars, these few early-type stars do not affect the disk fractions in a severe way (van der Marel & Pinilla 2023). Nevertheless, it might influence the estimates of the initial disk fraction and should be investigated in this context further.

Above, we showed that the spread in disk lifetimes remains even when concentrating on this specific stellar mass range. We investigate the role of stellar mass on the disk lifetime distribution in detail in S. Pfalzner & F. Dincer (2023, in preparation).

5.2. Initial Disk Properties

The masses of disks surrounding similar-aged stars can vary by orders of magnitude (e.g., Pascucci et al. 2016; Ansdell et al. 2017; Eisner et al. 2018; Cazzoletti et al. 2019; Cieza et al. 2019; Tobin et al. 2020; Tychoniecet al. 2020; Grant et al. 2021; Appelgren et al. 2023), even if the stars are of the same mass. This diversity in disk masses was found in gas and dust masses alike. Similarly, it has been shown that the total disk masses in a cluster decrease with cluster age (Andrews 2020). Thus, the broad disk lifetime distribution could reflect the differences in initial disk masses. Disks of low mass would be faster accreted and more easily dispersed than high-mass disks. This answer is only partially satisfying because it replaces the question of the origin of the disk lifetimes with that of the diversity of disk masses. Besides, some old disks (>10 Myr) still have relatively high disk masses.

Michel et al. (2021) suggest that the degree of structuring is crucial for the disk lifetime. They propose that two classes of disks, structured and unstructured, exist. The unstructured disks lose their dust masses quickly, whereas in structured disks dust traps allow for the formation of planetesimal belts at large radii, slowing down mass loss. The observation that structured protostellar disks are brighter and more extensive than unstructured disks supports this suggestion (Michel et al. 2021). However, the problem of resolving structure in low-mass disks might introduce a bias here.

5.3. Environment

The environment can also influence the disk lifetime (e.g., Adams et al. 2006). In regions of high stellar density, close flybys can truncate disks and, in extreme cases, even annihilate them (e.g., Olczak et al. 2010; Vincke & Pfalzner 2016; Winter et al. 2020; Cuello et al. 2023). If the environment is dense, relatively gas free, and contains high-mass stars, the radiation of these high-mass stars can destroy the disks around stars in their vicinity (e.g., Owen et al. 2010; Sellek et al. 2020; Concha-Ramírez et al. 2021; Parker et al. 2021; Winter & Haworth 2022). However, the main clusters in our study, Upper Sco and UCL/LLC, have a relatively low stellar density. Currently, stellar flybys and external photoevaporation likely play only a minor role in disk lifetime diversity. However, both clusters might have once been much denser (Pfalzner & Kaczmarek 2013). Thus, it can not be excluded that the once denser environment might be responsible for the short end of the disk lifetime distribution.

Even in low-density environments, about 10% of stars are likely to experience close flybys (Pfalzner et al. 2022). Thus, the environment may lead to premature disk dispersal in about 10% of stars.

5.4. Planet Formation

If the planet formation is very efficient in converting the disk's gas and dust into one or more planets, this might reduce the disk mass so much that the remnant material is quickly dispersed. Such a process of premature disk dispersal would be particularly efficient if a massive gas giant is formed. Planet formation by gravitational instability would be one way to form planets fast (Boss 1997). Another process that could trigger a planet's early and fast formation in a disk is the presence of interstellar objects as seeds for planet formation (Pfalzner & Govind 2021).

5.5. Stellar Binarity

The presence of a companion star influences the disk properties and frequency. A companion can prevent disk formation, limit its lifetime, or truncate it (Harris et al. 2012). Further, binaries can clear a cavity of 2–5 times the binary separation (Artymowicz & Lubow 1994; Hirsh et al. 2020; van der Marel & Mulders 2021). These effects lead to a lower disk fraction around close binary stars compared to single stars (Kraus et al. 2012). Besides, disks surrounding binary stars tend to be smaller (Akeson et al. 2019). The binarity of stars is known to increase with stellar mass (Raghavan et al. 2010) and still changes during the first 10 Myr within the host cluster of the stars (Kaczmarek et al. 2011; Korntreff et al. 2012). Thus, significant uncertainties exist concerning the binary fraction around low-mass stars younger than 10 Myr.

This study was limited to low-mass stars, which typically have a binary fraction of ≈20 %. If close binaries prohibit disk formation in some cases, then stellar binarity may play a

role in the initial disk fraction. If binarity is the primary mechanism for reducing the initial disk fraction, then the initial disk fraction should be smaller for higher-mass stars. Determining whether the initial disk fraction declines with stellar mass should be able to quantify the relevance of binarity in this context.

Binarity may also contribute to the portion of disks with relatively short disk dissipation times. We can estimate from our distribution how disk lifetime would be affected by binarity. Assuming 20% of stars have shorter disk lifetimes than average solely due to their binarity means that 20% of stars would have a disk lifetime significantly shorter than 5–10 Myr. Thus, the median disk lifetime of low-mass binary stars would be 1–2 Myr shorter than those of single stars. However, we find it unlikely that a single cause is responsible for the shorter-than-average disk lifetimes.

The processes described in Sections 5.1–5.5 might influence a particular disk's lifetime. However, the relative importance of the different mechanisms for shaping the disk lifetime distribution still needs further exploration.

6. Why the Lifetime Distribution Matters

Mean or median disk lifetimes have been used for more than 20 yr to restrict the time available for planet formation. Nevertheless, the more than 20 Myr old protoplanetary disks show that shifting toward a description by a disk lifetime distribution is long overdue. Such a disk lifetime distribution goes beyond acknowledging that a wide diversity exists in disk lifetimes. It quantifies the relative occurrence rate of very-short-lived and very-long-lived disks. Proceeding to a disk lifetime distribution approach affects mainly two research areas.

First, disk dispersal theory must account for the spread in disk lifetimes. Several theoretical works have recently investigated how the disk lifetime depends on stellar mass (Coleman & Haworth 2022; Wilhelm & Portegies Zwart 2022). These agree with observations showing such a mass dependence. However, the question is whether the disk lifetime spread is primarily due to the stellar mass dependence. Our results show that the diversity of disk lifetimes remains when concentrating on just low-mass stars.

Numerical investigations of disk dispersal often consider several of the many disk dispersal mechanisms. However, a match between simulation results and the here-derived disk lifetime distribution does not necessarily prove that the model is realistic. The problem is that there are many free parameters in these simulations, e.g., the α-viscosity, accretion rate, initial disk mass, and size. There is some risk that a match between the simulations and the distribution suffers from a posteriori treatment. Several combinations of these free parameters likely lead to a good match with the simulations. Therefore, ab initio simulations are more suitable for a comparison with the disk lifetime distribution. These a priori models provide the chance for a deeper understanding of the underlying dispersal mechanism(s). They start out with a very limited number of assumptions, and the initial conditions are well-defined by observations. Therefore, these models require few free parameters. Simply selecting parameters that match the distribution should be avoided, as these a posteriori approaches remain on a purely heuristic level.

Second, many planet formation models assume a specific typical disk lifetime. In the past, this was often in the 2–3 Myr range, or at least <10 Myr. Disks existing for more than 10 Myr have attracted relatively little attention. Realizing that at least the disks around low-mass stars persist on average longer (5–10 Myr) affects planet formation models. This change in perspective also applies to the width of the disk lifetime distribution.

Disks with different lifetimes likely directly influence the resulting planets and planetary systems. For example, assuming the standard formation channel for a typical gas giant takes 8 Myr. Then, early disk dispersal would stop the gas accretion process prematurely. The result would be a smaller gas envelope and core-to-gas ratio compared to the standard scenario. This example illustrates how short disk lifetimes could affect the type of planet forming. By contrast, long disk lifetimes affect the number of planets forming, and thus the planetary system structure. An explicit scenario is the following: In slowly forming planetary systems, the formation of one planet can induce spiral arms. In these spiral arms, the gas and dust density is enhanced, which can trigger the formation of additional planets. Unfortunately, the dependence of planet formation on disk lifetimes is challenging to test observationally.

7. Conclusion

The discovery of protoplanetary disks older than 20 Myr implies a large diversity in disk lifetimes. Some disks exist for just a few million years, while others live for dozens of millions of years. This finding implies that mean disk lifetimes provide limited information for disk development in general. Here, we introduced a new method for determining the disk lifetime distribution. Such a disk lifetime distribution can function as an input for planet formation theory. In addition, it provides a stringent test for existing disk dispersal theories.

We determine the disk lifetime distribution based on the disk frequencies of clusters of different ages. We concentrated on low-mass stars (spectral types M3.7–M6, $M_s \approx$ 0.1–0.25 $M_\odot$) in nearby (<200 pc) clusters and associations. The reason is that disk lifetimes depend on stellar mass. We want to exclude this dependency (Michel et al. 2021; Pfalzner et al. 2022). Among the clusters of the sample, Upper Sco and UCL/LLC are especially relevant as their large number of stars provides a high statistical significance (Luhman 2022a). We tested Gaussian, gamma, log-normal, Weibull, log-logistic, and beta distributions for their ability to provide a heuristic fit to the observational data.

If all stars were initially surrounded by a disk, meaning $f(t=0) = 100\%$, the disk lifetime distribution could be best described by a Weibull distribution with $k = 1.78$ and $\lambda = 9.15$. This left-skewed distribution shows a median disk lifetime $t_d = 8.1$ Myr, with most disks dissipating at the age of $t_{\max} = 7.21$ Myr. However, we generally find that fits with initial disk fractions <100% lead to a better match to the observational data. This finding agrees with the result of Michel et al. (2021). We obtain the best fit for an initial disk fraction of 65%. A Weibull distribution with $k = 2.34$ and $\lambda = 11.22$ and a Gaussian distribution with $\sigma = 5.04$ and $\mu = 9.52$ both lead to similar good approximations for the disk lifetime distribution. For the Weibull distribution, the corresponding median disk lifetime is 9.93 Myr and the maximum of the distribution is 8.83 Myr.

This work is the first step in determining the disk lifetime distribution. One critical point is that the derived disk lifetime distribution is dominated by two clusters: Upper Sco and UCL/LCC. Future improvements rely on more and better disk fraction data becoming available for clusters in the age range 3–15 Myr. These data must be statistically significant, meaning each sample should contain >200 stars. A major challenge will be better constraining the disk fraction at cluster age $t = 0$.

Independent of the tested type, all distributions are extensive with $\sigma > 6$ Myr in each case. Understanding the underlying reason for this large width is crucial for a deeper understanding of the disk dispersal mechanism. The broad distribution of disk lifetimes is likely one of the main reasons for the diversity of planetary systems.

Acknowledgments

We thank the referee for the valuable suggestions on improving the manuscript. This work was supported by the Ministry of Culture and Science of the State of North Rhine-Westphalia" as part of the profile-building project “Big Bang to Big Data”.

Appendix

Table 3 provides the parameters for the best-fit distributions of the different distribution types. The corresponding D values are given in Table 4. Table 5 defines test models accounting for the error bars of the disc fraction and age values of Upper Sco and UCL/LLC.

Table 4
Deviations of Different Distributions

Type	D(100%)	D (80%)	D (65%)
Gaussian	0.0564	0.0424	0.0302
Gamma	0.0828	0.0558	0.0603
Log-normal	0.0873	0.0579	0.0368
Weibull	0.0769	0.0523	0.0340
Log-logistic	0.0886	0.0582	0.0356
Beta	0.0815	0.0552	0.0356

Note. Column (1) indicates the distribution type, and columns (2)–(4) show the D values corresponding to the distributions listed in Table 3.

Table 5
Fit Parameters for the Various Distributions

ID	Disk Fractions		Cluster Ages		Gamma		Beta		Log-normal		Weibull		Log-logistic	
ID	f_{USco}	$f_{\mathrm{U/L}}$	t_{USco}	$t_{\mathrm{U/L}}$	$\bar{t_d}$	$\sigma(t_d)$	$\bar{t_d}$	$\sigma(t_d)$	$\bar{t_d}$	$\sigma(t_d)$	$\bar{t_d}$	$\sigma(t_d)$	$\bar{t_d}$	$\sigma(t_d)$
$L1_{100}$	0.25	0.09	11.0	15.0	8.5	20.6	8.4	20.8	8.9	19.4	8.1	22.4	9.3	24.8
$L2_{100}$	0.22	0.09	11.0	17.0	7.3	46.7	⋯	⋯	8.2	53.1	7.3	46.6	8.8	140.3
$L1_{80}$	0.25	0.09	11.0	15.0	9.4	19.9	9.3	20.1	9.8	19.2	9.0	21.7	10.0	25.5
$L2_{80}$	0.22	0.09	11.0	17.0	8.5	48.7	8.3	47.0	9.2	55.6	8.4	48.3	9.8	135.2
$L3_{100}$	0.25	0.09	12.0	15.0	9.8	13.3	9.8	13.6	10.1	12.2	9.3	16.2	10.4	13.8
$L4_{100}$	0.22	0.11	11.0	15.0	7.5	36.8	7.3	36.0	8.2	39.9	7.3	36.8	8.7	80.8

ORCID iDs

Susanne Pfalzner https://orcid.org/0000-0002-5003-4714
Furkan Dincer https://orcid.org/0009-0009-8603-9566

References

Adams, F. C., Proszkow, E. M., Fatuzzo, M., & Myers, P. C. 2006, ApJ, 641, 504
Akeson, R. L., Jensen, E. L. N., Carpenter, J., et al. 2019, ApJ, 872, 158
Andrews, S. M. 2020, ARA&A, 58, 483
Ansdell, M., Williams, J. P., Manara, C. F., et al. 2017, AJ, 153, 240
Appelgren, J., Lambrechts, M., & van der Marel, N. 2023, A&A, 673, A139
Artymowicz, P., & Lubow, S. H. 1994, ApJ, 421, 651
Ballabio, G., Nealon, R., Alexander, R. D., et al. 2021, MNRAS, 504, 888
Boss, A. P. 1997, Sci, 276, 1836
Briceño, C., Calvet, N., Hernández, J., et al. 2019, AJ, 157, 85
Carpenter, J. M., Mamajek, E. E., Hillenbrand, L. A., & Meyer, M. R. 2006, ApJL, 651, L49
Cazzoletti, P., Manara, C. F., Liu, H. B., et al. 2019, A&A, 626, A11
Cieza, L. A., Ruíz-Rodríguez, D., Hales, A., et al. 2019, MNRAS, 482, 698
Coleman, G. A. L., & Haworth, T. J. 2022, MNRAS, 514, 2315
Concha-Ramírez, F., Wilhelm, M. J. C., Portegies Zwart, S., van Terwisga, S. E., & Hacar, A. 2021, MNRAS, 501, 1782
Cuello, N., Ménard, F., & Price, D. J. 2023, EPJP, 138, 11
de Geus, E. J., de Zeeuw, P. T., & Lub, J. 1989, A&A, 216, 44
Dickson-Vandervelde, D. A., Wilson, E. C., & Kastner, J. H. 2021, AJ, 161, 87
Eisner, J. A., Arce, H. G., Ballering, N. P., et al. 2018, ApJ, 860, 77
Emsenhuber, A., Burn, R., Weder, J., et al. 2023, A&A, 673, A78
Ercolano, B., & Pascucci, I. 2017, RSOS, 4, 170114
Fedele, D., van den Ancker, M. E., Henning, T., Jayawardhana, R., & Oliveira, J. M. 2010, A&A, 510, A72
Forgan, D., & Rice, K. 2013, MNRAS, 432, 3168
Galli, P. A. B., Bouy, H., Olivares, J., et al. 2021a, A&A, 654, A122
Galli, P. A. B., Bouy, H., Olivares, J., et al. 2021b, A&A, 646, A46
Grant, S. L., Espaillat, C. C., Wendeborn, J., et al. 2021, ApJ, 913, 123
Haisch, K. E. J., Lada, J., & Lada, C. J. 2001, ApJL, 553, L153
Harris, R. J., Andrews, S. M., Wilner, D. J., & Kraus, A. L. 2012, ApJ, 751, 115
Hernández, J., Hartmann, L., Calvet, N., et al. 2008, ApJ, 686, 1195
Hernández, J., Hartmann, L., Megeath, T., et al. 2007, ApJ, 662, 1067
Hirsh, K., Price, D. J., Gonzalez, J. F., Ubeira-Gabellini, M. G., & Ragusa, E. 2020, MNRAS, 498, 2936
Ida, S., & Lin, D. N. C. 2010, ApJ, 719, 810
Kaczmarek, T., Olczak, C., & Pfalzner, S. 2011, A&A, 528, A144
Kennedy, G. M., Matrà, L., Facchini, S., et al. 2019, NatAs, 3, 230
Kenyon, S. J., & Hartmann, L. 1995, ApJS, 101, 117
Korntreff, C., Kaczmarek, T., & Pfalzner, S. 2012, A&A, 543, A126
Kraus, A. L., Ireland, M. J., Hillenbrand, L. A., & Martinache, F. 2012, ApJ, 745, 19
Kunitomo, M., Suzuki, T. K., & Inutsuka, S. i. 2020, MNRAS, 492, 3849
Lee, J., Song, I., & Murphy, S. 2020, MNRAS, 494, 62
Luhman, K. L. 2022a, AJ, 163, 25
Luhman, K. L. 2022b, AJ, 163, 24
Luhman, K. L. 2023a, AJ, 165, 37
Luhman, K. L. 2023b, AJ, 165, 269
Luhman, K. L., & Esplin, T. L. 2020, AJ, 160, 44
Manzo-Martínez, E., Calvet, N., Hernández, J., et al. 2020, ApJ, 893, 56
Michel, A., van der Marel, N., & Matthews, B. 2021, ApJ, 921, 72
Mordasini, C., Alibert, Y., Benz, W., & Naef, D. 2009, A&A, 501, 1161
Mordasini, C., Alibert, Y., Benz, W., Klahr, H., & Henning, T. 2012, A&A, 541, A97
Murphy, S. J., Mamajek, E. E., & Bell, C. P. M. 2018, MNRAS, 476, 3290
Olczak, C., Pfalzner, S., & Eckart, A. 2010, A&A, 509, A63
Owen, J. E., Ercolano, B., Clarke, C. J., & Alexander, R. D. 2010, MNRAS, 401, 1415
Parker, R. J., Alcock, H. L., Nicholson, R. B., Panić, O., & Goodwin, S. P. 2021, ApJ, 913, 95
Pascucci, I., Testi, L., Herczeg, G. J., et al. 2016, ApJ, 831, 125
Pecaut, M. J., Mamajek, E. E., & Bubar, E. J. 2012, ApJ, 746, 154
Pfalzner, S. 2022, RNAAS, 6, 219
Pfalzner, S., Dehghani, S., & Michel, A. 2022, ApJL, 939, L10
Pfalzner, S., & Govind, A. 2021, ApJ, 921, 90
Pfalzner, S., & Kaczmarek, T. 2013, A&A, 559, A38
Pfalzner, S., Steinhausen, M., & Menten, K. 2014, ApJL, 793, L34
Preibisch, T., Brown, A. G. A., Bridges, T., Guenther, E., & Zinnecker, H. 2002, AJ, 124, 404
Raghavan, D., McAlister, H. A., Henry, T. J., et al. 2010, ApJS, 190, 1
Ratzenböck, S., Alves, J., Großschedl, J. E., et al. 2023, A&A, 678, A71
Ribas, Á., Bouy, H., & Merín, B. 2015, A&A, 576, A52
Ribas, Á., Merín, B., Bouy, H., & Maud, L. T. 2014, A&A, 561, A54
Richert, A. J. W., Getman, K. V., Feigelson, E. D., et al. 2018, MNRAS, 477, 5191
Roccatagliata, V., Bouwman, J., Henning, T., et al. 2011, ApJ, 733, 113
Ronco, M. P., Guilera, O. M., Cuadra, J., et al. 2021, ApJ, 916, 113
Schlecker, M., Burn, R., Sabotta, S., et al. 2022, A&A, 664, A180
Sellek, A. D., Booth, R. A., & Clarke, C. J. 2020, MNRAS, 492, 1279
Silverberg, S. M., Kuchner, M. J., Wisniewski, J. P., et al. 2016, ApJL, 830, L28
Silverberg, S. M., Wisniewski, J. P., Kuchner, M. J., et al. 2020, ApJ, 890, 106
Spezzi, L., Petr-Gotzens, M. G., Alcalá, J. M., et al. 2015, A&A, 581, A140
Sullivan, K., & Kraus, A. L. 2021, ApJ, 912, 137
Tobin, J. J., Sheehan, P. D., Megeath, S. T., et al. 2020, ApJ, 890, 130
Tychoniec, L., Manara, C. F., Rosotti, G. P, et al. 2020, A&A, 640, A19
van der Marel, N., & Mulders, G. D. 2021, AJ, 162, 28
van der Marel, N., & Pinilla, P. 2023, arXiv:2310.09077
van Terwisga, S. E., Hacar, A., van Dishoeck, E. F., Oonk, R., & Portegies Zwart, S. 2022, A&A, 661, A53
Vincke, K., & Pfalzner, S. 2016, ApJ, 828, 48
Wilhelm, M. J. C., & Portegies Zwart, S. 2022, MNRAS, 509, 44
Williams, J. P., & Cieza, L. A. 2011, ARA&A, 49, 67
Winter, A. J., & Haworth, T. J. 2022, EPJP, 137, 1132
Winter, A. J., Kruijssen, J. M. D., Chevance, M., Keller, B. W., & Longmore, S. N. 2020, MNRAS, 491, 903
Wyatt, M. C., Panić, O., Kennedy, G. M., & Matrà, L. 2015, Ap&SS, 357, 103
Yasui, C., Kobayashi, N., Tokunaga, A. T., & Saito, M. 2014, MNRAS, 442, 2543